6-2002

The Melting Lines of Model Systems Calculated from Coexistence Simulations

James R. Morris
Iowa State University

Xueyu Song
Iowa State University, xsong@iastate.edu

The Melting Lines of Model Systems Calculated from Coexistence Simulations

Abstract

We have performed large-scale molecular dynamics simulations of coexisting solid and liquid phases using $4\varepsilon(\sigma/r)n$ interactions for n=9 and n=12, and for Lennard-Jones systems, in order to calculate the equilibrium melting curve. The coexisting systems evolve rapidly toward the melting temperature. The P–Tmelting curves agree well with previous calculations, as do the other bulk phase properties. The melting curve for the Lennard-Jones system, evaluated using various truncations of the potential, converges rapidly as a function of the potential cutoff, indicating that long-range corrections to the free energies of the solid and liquid phases very nearly cancel. This approach provides an alternative to traditional methods of calculating melting curves.

Disciplines

Chemistry

The melting lines of model systems calculated from coexistence simulations

James R. Morris and Xueyu Song

The melting lines of model systems calculated from coexistence simulations

James R. Morris[a)]

Metal and Ceramic Sciences Program, Ames Laboratory (USDOE), Iowa State University, Ames, Iowa 50011

Xueyu Song

Department of Chemistry, Iowa State University, Ames, Iowa 50011

We have performed large-scale molecular dynamics simulations of coexisting solid and liquid phases using $4\epsilon(\sigma/r)^n$ interactions for $n=9$ and $n=12$, and for Lennard-Jones systems, in order to calculate the equilibrium melting curve. The coexisting systems evolve rapidly toward the melting temperature. The $P-T$ melting curves agree well with previous calculations, as do the other bulk phase properties. The melting curve for the Lennard-Jones system, evaluated using various truncations of the potential, converges rapidly as a function of the potential cutoff, indicating that long-range corrections to the free energies of the solid and liquid phases very nearly cancel. This approach provides an alternative to traditional methods of calculating melting curves. © *2002 American Institute of Physics.* [DOI: 10.1063/1.1474581]

I. INTRODUCTION

The calculation of the melting line of materials is of fundamental interest,[1] representing a fundamental understanding of the equilibrium properties of both the solid and liquid phases, and the competition between them. Traditionally, these calculations have been made using free energy calculations: by calculating the Gibbs free energy of both phases, the melting line may be determined directly[1] using the relationship

$$g_s(P,T_m)=g_l(P,T_m), \tag{1}$$

where $g(P,T)$ is the Gibbs free energy per particle (with the subscripts s and l indicating the solid and liquid phases, respectively) and $T_m(P)$ is the melting temperature at a given pressure. The difficulty in the direct application of this is that the free energy is not trivially calculated. Typically, many simulations are required in order to calculate the difference in free energy from a reference system to the system of interest at some pressure and temperature, and then to map out the Gibbs free energy as a function of pressure and temperature. Although the Gibbs–Duhem integration method[2,3] helps with this approach, a starting point, which is usually obtained from traditional thermodynamic integration, is still required.

An alternative is to simulate the coexistence directly with an explicit interface. This strategy had been used in the 1970s, but the calculated coexistence properties are not accurate compared with the thermodynamic integration due to small system size and short simulation time.[4–6] Recently, with much larger system sizes and longer simulation times, melting temperatures have been calculated directly by simulating coexisting liquid and solid phases with molecular dynamics,[7,8] utilizing the fact that a system with both phases will evolve toward the equilibrium melting point. Typically, the system evolves in a constant volume, particle number, and energy ensemble (NVE). In this case, we may understand the evolution in a straightforward fashion. If the system initially has a temperature higher than the melting temperature, then some of the solid phase will melt. This requires latent heat, and therefore converts some of the kinetic energy into potential energy, reducing the temperature. Thus, the system approaches the melting temperature from above. A similar argument shows that if the initial temperature is too low, it will evolve toward the melting temperature from below. This approach is not limited to an NVE ensemble, but may be easily generalized.

The accuracy of the direct approach has not been completely established, especially for systems for which reliable calculations have been made. In this paper, we demonstrate the approach for purely repulsive $4\epsilon(\sigma/r)^n$ systems with $n=9$ and $n=12$, and for the Lennard-Jones (LJ) interaction, which are well-studied condensed systems.[9–12] In both cases, the results agree well with previous calculations.[11,12] We note that there are potential complications associated with the long tail of the LJ potential. Simulations with the full potential are prohibitively long, but truncation of the potential could (in principle) have a significant effect on the melting line, and therefore require corrections. We show that the melting line is surprisingly robust: truncation of the potential at distances as short as 2.1σ has a minimal effect on the melting line.

II. TECHNIQUE

We begin by discussing the various model interactions used in this paper, and how we have truncated them smoothly in order to minimally affect the potential. The LJ interaction is specified by

---

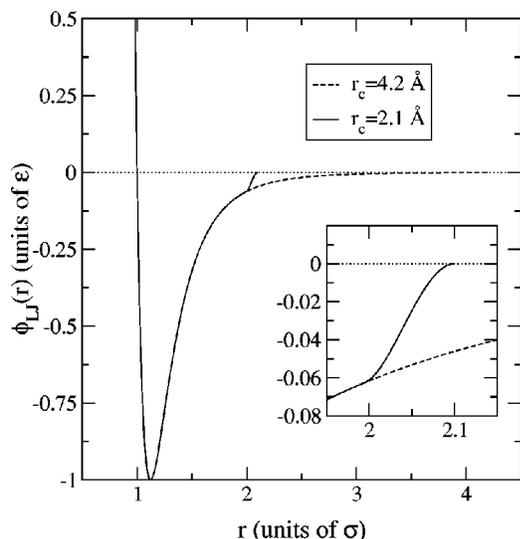[a)]Electronic mail: jrmorris@ameslab.gov

FIG. 1. The truncated LJ potential energy function for $r_c = 2.1\sigma$ and $r_c = 4.2\sigma$. The truncation of the potential for the shorter cutoff distance is apparent; in the inset, we show the potential in the region $r_m \leq r \leq r_c$ to demonstrate that the potential and its derivatives are continuous.

$$\phi_{LJ}(r) = 4\epsilon\left[\left(\frac{\sigma}{r}\right)^{12} - \left(\frac{\sigma}{r}\right)^{6}\right]. \qquad (2)$$

In Eq. (2), ϵ specifies an energy scale, and σ specifies a length scale. Similarly, we define the purely repulsive "soft-core" potentials by

$$\phi_n(r) = 4\epsilon\left(\frac{\sigma}{r}\right)^{n}, \qquad (3)$$

where we have included the factor of 4 in front in order to compare with the LJ system and with previous results.[12] This factor can easily be absorbed into the energy scale ϵ.

We also define a cutoff function so that the potentials will be unaltered for distances less than a chosen distance r_m, and go smoothly to zero at distances greater than r_c. We do this using the truncation method used in Ref. 13. We first define $x = (r - r_m)/(r_c - r_m)$, so that the potential is unaltered when $x < 0$ and is 0 when $x \geq 1$. Then the cutoff function is chosen to be

$$f(x) = \begin{cases} 1, & x < 0 \\ 1 - 3x^2 + 2x^3, & 0 \leq x < 1 \\ 0, & x \geq 1 . \end{cases} \qquad (4)$$

The function $f(r)$ goes smoothly from 1 to 0 between the points r_m and r_c. We have chosen $r_m = 0.95 r_c$. We then perform simulations using the strictly short-range potential

$$\tilde{\phi}(r) = \phi(r)f(r). \qquad (5)$$

In order to test how various ranges of interactions affect the results, we have performed the calculation of the LJ phase diagram using three values of the cutoff: $r_c/\sigma = 2.1$, 4.2, and 8.0. We show the graphs of $\tilde{\phi}_{LJ}(r)$ for the first two of these in Fig. 1. As we see, the shortest cutoff is quite dramatic. For the soft-core repulsive potentials, we have cho-
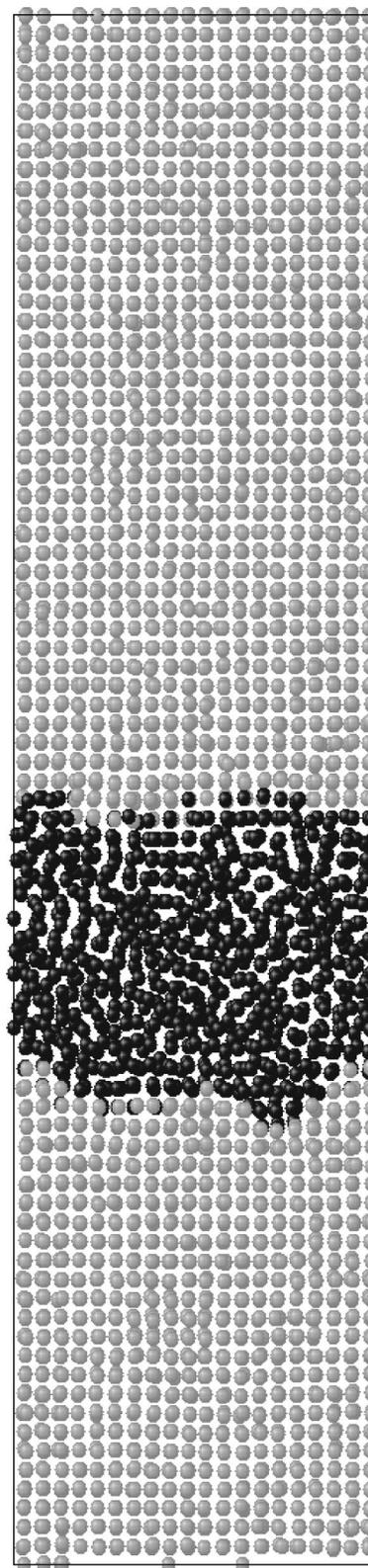
FIG. 2. A snapshot of a simulated coexisting LJ system, with a temperature $T = 2.2\epsilon$ and a total density of $N/V = 1.1495/\sigma^3$ (intermediate between the solid and liquid densities). Solid atoms (as determined by the order parameter described in the text) are dark, while liquid atoms are light.

sen $r_c = 2.5\sigma$ for $n = 9$ and $r_c = 2.0\sigma$ for $n = 12$. In this case, the potentials are less than 0.002ϵ at r_m. We have not tested in detail the effects of the cutoff for the soft core potentials; given that the results for the LJ potential converge rapidly

FIG. 3. The order parameter vs position along the direction z normal to the interfaces, for the atoms shown in Fig. 2. The solid region extends from $z \approx -10\sigma$ to $z \approx 10\sigma$, where the order parameter is largest.

FIG. 5. The pressure–temperature diagram for the LJ system. We have included results for all cutoffs of the LJ potential. The solid line is the fit from the results of Ref. 12, while the large open squares indicate the results of Ref. 9. Error bars for the calculations are approximately equal to the symbol size.

with cutoff distance (as we demonstrate in the following), and that the LJ potential has a tail that is significantly larger range than the soft-core potentials examined here, we believe that our results for the soft-core potential are essentially converged.
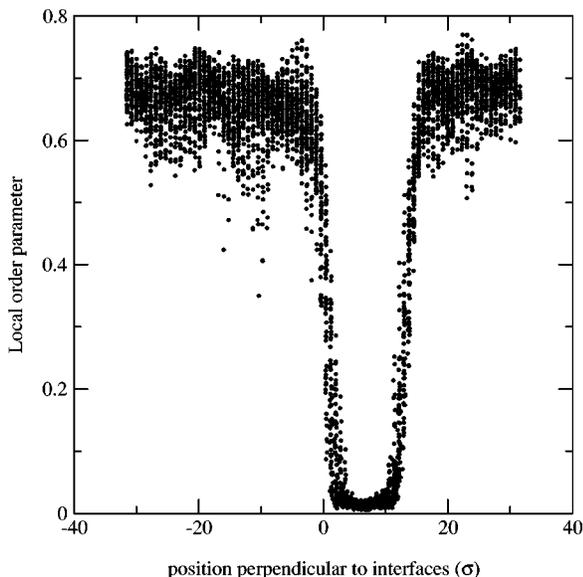
To begin the simulations, a simulation of the solid is first performed near the estimated melting temperature, to achieve an approximate equilibrated initial condition. Next, a liquid system is created, by combining large amplitude random displacements of the solid phase with a high temperature simulation ($\sim 50\%$ above the melting temperature). The
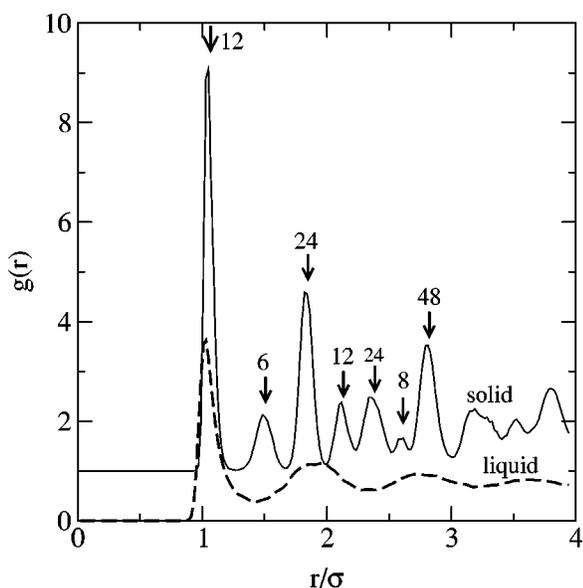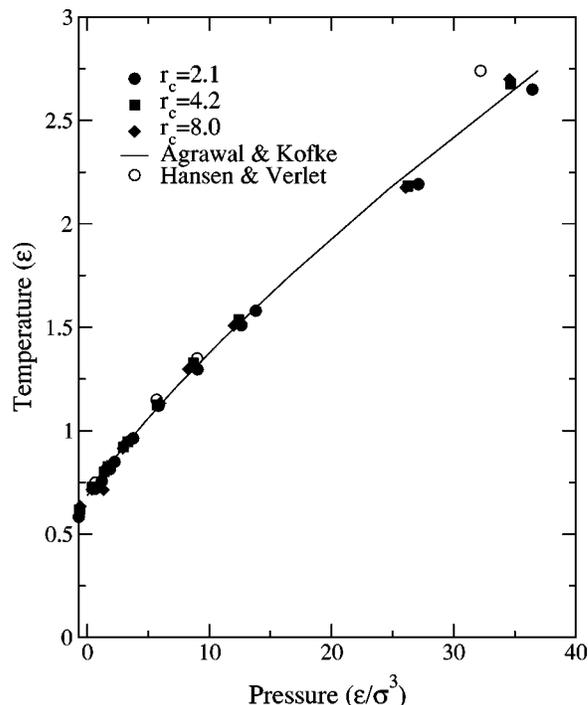

FIG. 4. The pair distribution function $g(r)$ calculated separately for the solid and the liquid atoms shown in Fig. 2. The solid phase $g(r)$ curve has been shifted upward for clarity. For the solid phase, the positions and coordination number for different neighboring shells of atoms is shown, based upon an ideal fcc lattice.

two systems are then brought into contact, by joining the two systems. Using fully periodic boundary conditions, this creates two interfaces between the solid and liquid systems. We then equilibrate the system briefly [10 000 molecular dynamics (MD) time steps] near the melting temperature, with the temperature being adjusted using velocity rescaling. The system is then allowed to equilibrate using a NVE ensemble (constant particle number, volume, and energy). As the system is closed, the temperature and pressure will evolve. If the system is close to coexisting conditions, it naturally evolves to the equilibration. On the other hand, if the energy is too high (or too low), the system will melt (or solidify) completely. The time required to equilibrate depends upon the size of the system, and on the difference between the initial and equilibrium conditions. Once a coexisting simulation has been equilibrated, the coexisting conditions (average pressure and temperature) can be calculated, as well as the single phase properties (average internal energy and density). The system can then be perturbed by changing the volume and energy, and re-equilibrated, to calculating the coexisting properties at a different point in the phase diagram.

For most of the simulations presented here, we used a total of 16 000 atoms. However, it is important to note that this large number is not required for the coexisting simulations; in a previous work,[7] we used as few as 1024 atoms and achieved good results. The effects of system size are examined for one choice of parameters below; we find little change in melting temperature and pressures as the system size is varied from 2000 to 16 000 atoms.

We chose a molecular dynamics time step of 0.003 Δt,

TABLE I. Results for the Lennard-Jones melting pressures and temperatures, with various cutoffs of the potential.

$r_c = 2.1\sigma$		$r_c = 4.0\sigma$		$r_c = 8.0\sigma$	
P (ϵ/σ^3)	T (ϵ)	P (ϵ/σ^3)	T (ϵ)	P (ϵ/σ^3)	T (ϵ)
-0.685	0.584	-0.619	0.618	-0.568	0.634
0.632	0.718	0.426	0.727	0.380	0.715
1.201	0.756	1.409	0.801	1.326	0.803
1.858	0.814	1.729	0.827	1.641	0.828
2.192	0.838				
2.239	0.849	2.970	0.921	2.932	0.915
3.765	0.963	3.329	0.946	3.243	0.945
5.845	1.120	5.760	1.124	5.949	1.132
9.027	1.296	8.683	1.327	8.275	1.297
12.624	1.510	12.407	1.535	11.991	1.508
13.798	1.580				
27.118	2.192	26.207	2.182	26.064	2.177
36.445	2.650	34.671	2.676	34.573	2.700

where $\Delta t \equiv \sqrt{m\sigma^2/\epsilon}$, where m is the mass of an atom. This time step is sufficiently short that total energy is conserved to a high degree of accuracy. We typically used 100 000 time steps for the equilibration run, and another 50 000 for calculating the average thermodynamic properties.

III. RESULTS

We show a picture from the simulations in Fig. 2. We see that the system contains well-defined regions of solid and liquid, with a fairly sharp transition region between them. The atomic planes in the solid phase are clearly seen. In the Fig. 2, the interfacial plane has an average orientation along the [001] direction; however, it is clear that the interface is not faceted, but instead is rough. The roughness of the interface is a measure of the interfacial stiffness of the system.[14,15] In the Fig. 2, we have defined atoms as being in an instantaneous "solid" or "liquid" configuration. To do this, we define a local order parameter that provides a measure of local fcc order. For this, we choose a set of N_q wave vectors $\{\mathbf{q}_i\}$ such that

$$\exp(i\mathbf{q}\cdot\mathbf{r}) = 1 \tag{6}$$

for any vector $\mathbf{r}$ connecting near neighbors in a perfect fcc lattice. We omit one of each pair of antiparallel wave vectors; thus, $N_q = 6$. We then define the local order parameter as

$$\psi = \left| \frac{1}{N_q} \frac{1}{Z} \sum_{\mathbf{r}} \sum_{\mathbf{q}} \exp(i\mathbf{q}\cdot\mathbf{r}) \right|^2 , \tag{7}$$

where the sum on $\mathbf{r}$ runs over each of Z neighbors found within a distance r_c of the atom, chosen to be between the first and second neighbor shells in the perfect lattice.

While Eq. (7) is reasonably good at producing an order parameter that is small for the liquid phase and large for the solid phase, we have found a couple of methods that improve how well we can discriminate between these phases. First of all, instantaneous atomic positions include significant amounts of fast atomic vibrations that reduce the order of the solid phase. To overcome this, we average the atomic positions over short periods of time (100 MD time steps), pro-

ducing significantly more order in the solid phase. Second, we calculate an *average* order parameter $\bar{\psi}$ for each atom, by averaging over the neighboring values:

$$\bar{\psi}_i = \frac{1}{Z+1} \left(\psi_i + \sum_j \psi_j \right), \tag{8}$$

where j runs over all Z neighbors of atom i.

To demonstrate the effectiveness of Eq. (8), Fig. 3 shows the values of $\bar{\psi}$ for each atom shown in Fig. 2, as a function of distance along an axis oriented perpendicular to the interface. As seen in the Fig. 3, the liquid region has order parameters with $\bar{\psi} < 0.05$, while the solid region has atoms with order parameters usually satisfying $\bar{\psi} > 0.2$. The two regions are clearly identifiable, and there are very few atoms away from the interface that have values satisfying $0.05 < \bar{\psi} < 0.2$. In Fig. 2, we have defined all atoms with $\bar{\psi} > 0.08$ as "solid," and the remaining atoms as liquid. This designation is for demonstration purposes only, and plays no role in our evaluation of the properties of the coexisting system. As a separate test of this designation, and to demonstrate that these two distinct regions have properties closely reproducing the separate, homogeneous liquid and solid phases, we have calculated the pair correlation function $g(r)$ separately for the two regions. The results, shown in Fig. 4, show that the liquid region has a pair correlation function typical of a homogeneous LJ liquid. The solid phase shows much more structure. We have labeled the $g(r)$ results for the solid

TABLE II. Melting temperatures as a function of pressure for the LJ system, determined by interpolating from Table I.

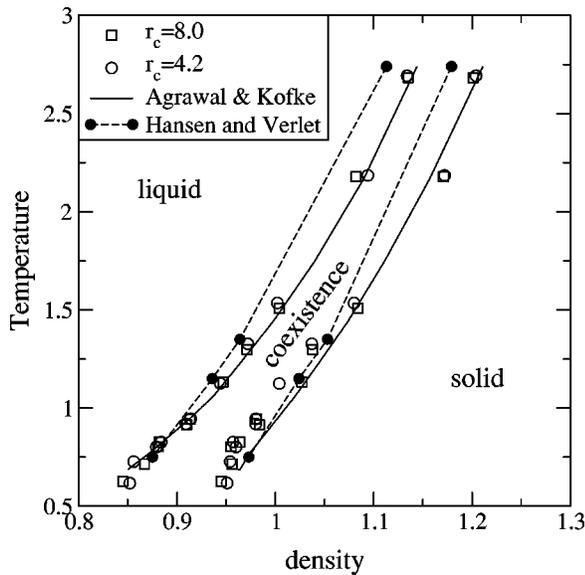| P (ϵ/σ^3)	T_m (ϵ), $r_c = 2.1\sigma$	T_m (ϵ), $r_c = 4.2\sigma$	T_m (ϵ), $r_c = 8.\sigma$
0.0	0.654	0.683	0.683
5.0	1.056	1.068	1.066
10.0	1.354	1.401	1.395
15.0	1.635	1.657	1.651
20.0	1.865	1.891	1.889
25.0	2.095	2.125	2.126
30.0	2.334	2.403	2.419
35.0	2.579	2.695	2.726

FIG. 6. The density–temperature relationship for the LJ system. We show our results for $r_c=4.2\sigma$ and $r_c=8.0\sigma$ as open symbols. Results from Ref. 12 are shown as solid lines, and those from Ref. 9 are shown as closed circles connected by dashed lines. Error bars for the calculations are approximately equal to the symbol size.

phase by calculating the position of neighboring shells of atoms from a fcc lattice, as well as the number of atoms in each shell. These positions and coordinations are indicated by the arrows in Fig. 4. There is a clear correlation between the position and heights of the peaks of $g(r)$ and the calculated neighboring shell distances and coordinations.

We begin by discussing the results for the LJ potential. Our primary results are shown in Fig. 5 and in Table I. In the Fig. 5, we have shown results for all three values of the cutoff distance. As we can see, the results for all three cutoff distances are in close agreement. We also show the results
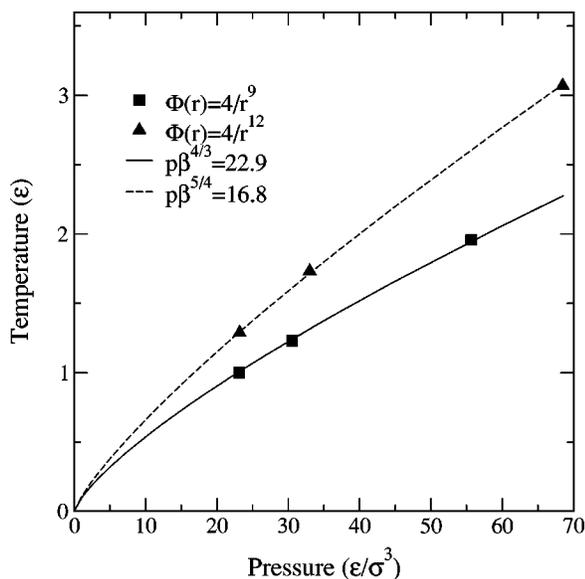

FIG. 7. The pressure–temperature diagram for the soft core systems. The dashed lines are fits to the soft-core results, to the form $p\beta^\nu=C$ with $\nu=\frac{4}{3}$ for $n=9$ and $\nu=\frac{5}{4}$ for $n=12$. Error bars for the calculations are approximately equal to the symbol size.

TABLE III. Melting pressures, temperatures, and coexisting densities scaled by $T_m^{1/3}$ for the soft core $n=9$ system.

P (ϵ/σ^3)	T_m (ϵ)	$\rho_{sol}/T_m^{1/3}$ (σ^{-3})	$\rho_{liq}/T_m^{1/3}$ (σ^{-3})
23.14	0.99	0.915	0.892
30.59	1.21	0.918	0.897
55.64	1.96	0.903	0.885

from Refs. 9 and 12. Our simulation results are in close agreement with the results of Ref. 12 at all densities, while the highest density result of Ref. 9 departs significantly from these calculations.

In Table I, it is difficult to see how the results converge as a function of the potential cutoff, as each simulation evolves to slightly different pressures and temperatures. To better demonstrate the rapid convergence, Table II shows the predicted melting temperatures at selected pressures, calculated by linear interpolation of the results given in Table I. Table II demonstrates that the results found using $r_c=2.1\sigma$ have a typical error of about 4% too low (compared to the largest value of r_c), while those using $r_c=4.2\sigma$ differ by less than 1%.

In Fig. 6 we show the phase diagrams for the LJ system as a function of density and temperature. We compare our results for $r_c=4.2\sigma$ and $r_c=8.0\sigma$ with those of Refs. 9 and 12. We see that our results are in very good agreement with those of Ref. 12, while those of Ref. 9 are off significantly, especially at higher pressures. The results for the liquid phase are particularly good. Our results for the solid phase show significant scatter, and suggest that at low pressures, the solid phase has a lower density than that predicted by Ref. 12.

In Fig. 7, we show the melting temperature for the soft core $n=9$ and $n=12$ systems for three different pressures. For the soft core systems, the equilibrium melting temperature and pressures should satisfy[9,10]

$$P\beta^\alpha=C_n, \tag{9}$$

where $\beta=1/k_BT$ and $\alpha=(3+n)/n$, and C_n is a constant. The results shown in Fig. 7 are consistent with this, with $C_9=22.90\pm0.03$ and $C_{12}=16.80\pm0.03$. These latter results are essentially consistent with the value of Ref. 12 found $C_{12}=16.89$, but somewhat higher than those of Ref. 9. The melting pressures and temperatures are given in Tables III and IV for the two systems. In Tables III and IV, we also show the coexisting solid and liquid densities, scaled by $T_m^{3/n}$. For a soft sphere system, these densities should scale with this behavior. As Tables III and IV demonstrate, our simulations closely agree with this scaling behavior.

TABLE IV. Melting pressures, temperatures, and coexisting densities scaled by $T_m^{1/4}$ for the soft core $n=12$ system.

P (ϵ/σ^3)	T_m (ϵ)	$\rho_{sol}/T_m^{1/4}$ (σ^{-3})	$\rho_{liq}/T_m^{1/4}$ (σ^{-3})
23.19	1.29	0.857	0.825
33.01	1.73	0.852	0.821
68.48	3.07	0.855	0.823

TABLE V. Melting pressures and temperatures for $r_c = 2.1\sigma$ cutoff LJ potential, calculated for various system sizes. We have also included the rms variation in temperature (ΔT) during the simulation.

N	P (ϵ/σ^3)	T_m (ϵ)	ΔT (ϵ)
2 000	1.195	0.760	0.0099
4 000	1.192	0.758	0.0071
8 000	1.197	0.756	0.0050
16 000	1.201	0.756	0.0038

In all of these results, we have used a large system size, with 16 000 atoms. This represents a significant computational effort, especially for the larger cutoff distance. However, such a large system size is not necessary. This has been demonstrated previously for a different potential.[7] We also test this for the LJ system, with the smallest cutoff ($r_c = 2.1\sigma$). We have performed simulations for $N = 2000$, 4000, 8000 and 16 000 atoms, keeping N/V fixed, and performing the simulations at a specific total energy per particle. We list the results in Table V. Table V clearly demonstrates that the numbers are very close, essentially independent of system size. We also define the variation in temperature during the simulation as

$$\Delta T \equiv \langle (T - \langle T \rangle)^2 \rangle^{1/2}$$

and find that this decreases with system size as $N^{-1/2}$ as expected.

IV. DISCUSSION

In this paper, we have calculated the melting curves of the LJ system, and of the soft-core potentials $\phi(r) = 4/r^9$ and $\phi(r) = 4/r^{12}$ using molecular dynamics simulations of the coexisting systems. We find good agreement with previous results. In particular, our phase diagram for the LJ system is close to that of Ref. 12. While the simulations performed here required a significant amount of computational effort, our system size studies demonstrate that this method does not require as large systems as required here. Moreover, the largest amount of effort was spent for the longest cutoff of the LJ system; as we have demonstrated here, the results are not sensitive to this cutoff. Presumably, this insensitivity is due to the relatively similar densities of the liquid and solid phases, and their small compressibility.

One difficulty in these simulations is that for the geometries used here, the system is not necessarily under hydrostatic pressure: the stresses may differ along different axes. We have treated this problem by manually adjusting the system box sizes of our initial simulations so that the different stress components are approximately equal, and calculating the average pressure $P = -\frac{1}{3}(\sigma_{xx} + \sigma_{yy} + \sigma_{zz})$ from the stress tensor σ_{ij}. This suffices for a small number of geometries, where this may be accomplished by hand fairly rapidly. Deviations from hydrostatic pressure are likely to be our largest source of error. This problem could be addressed by equilibrating under stress conditions, allowing the box shape to evolve to achieve hydrostatic conditions. An alternative would be to perform a simulation where the solid is completely bounded by liquid. In such a case, the system should naturally evolve toward hydrostatic conditions. However, this would likely require significantly larger numbers of atoms than are needed for the simpler geometry considered here.

An additional consideration is that the presence of the interface can produce stress in the system, even when the box size is optimized for the bulk crystal and liquid densities. This interface stress is due to the relaxations that the surface would like to undergo. However, we believe that this is small, in particular given the roughness of the interface. Where a flat interface may want to undergo relaxations or reconstructions to relieve the surface stress (as happens in crystal-vapor surfaces), the rough interface has sufficient "defects" to relieve most of such stress. For small systems, this may be more significant. Moreover, for very small systems, the crystal may eventually be sufficiently small that the free energy cost of the interface, and the stress from the interface, may outweigh the free energy gain of forming a solid region. In this case, the solid region may vanish entirely. We saw exactly this behavior in previous simulations.[7] This is also likely to be the origin of difficulties in early coexistence simulations.[4–6]

We note that this technique is generalizable to Monte Carlo simulations as well. This may be done using a NVT ensemble, under conditions when N/V is between the liquid and solid densities of the pure phases at the given temperature. This provides a restoring force that drives the system toward an equilibrium consisting of two phases. The approach is not as useful for solid-vapor or liquid-vapor phase diagrams: in MD, the equilibration time is not sufficiently long. For liquid-vapor phase diagrams, existing MC simulations using a Gibbs ensemble are better suited.[16,17] Within the MD simulations presented here, we may examine the melting curve into metastable regions, i.e., at pressures close to the triple point.

ACKNOWLEDGMENTS

[1] D. Frenkel and B. Smit, *Understanding Molecular Simulation*, 1st ed. (Academic, San Diego, 1996).
[2] D. A. Kofke, Mol. Phys. **78**, 1331 (1983).
[3] D. A. Kofke, Adv. Chem. Phys. **105**, 405 (1999).
[4] A. Ladd and L. Woodcock, Chem. Phys. Lett. **51**, 155 (1977).
[5] A. Ladd and L. Woodcock, Mol. Phys. **36**, 611 (1978).
[6] J. Cape and L. Woodcock, Chem. Phys. Lett. **59**, 274 (1978).
[7] J. R. Morris, C. Z. Wang, K. M. Ho, and C. T. Chan, Phys. Rev. B **49**, 3109 (1994).
[8] A. B. Belonoshko, R. Ahuja, and B. Johansson, Phys. Rev. Lett. **84**, 3638 (2000).

[9] J.-P. Hansen, Phys. Rev. A **2**, 221 (1970).

[10] W. G. Hoover, S. G. Gray, and K. W. Johnson, J. Chem. Phys. **55**, 1128 (1971).

[11] R. Agrawal and D. A. Kofke, Mol. Phys. **85**, 23 (1995).

[12] R. Agrawal and D. A. Kofke, Mol. Phys. **85**, 43 (1995).

[13] J. Mei and J. W. Davenport, Phys. Rev. B **46**, 21 (1992).

[14] J. R. Morris, Y. Y. Ye, Z. Y. Lu, and K. M. Ho, Interface Sci. (submitted); J. R. Morris, Phys. Rev. B (submitted).

[15] J. J. Hoyt, M. Asta, and A. Karma, Phys. Rev. Lett. **86**, 5530 (2001).

[16] A. Z. Panagiotopoulos, Mol. Phys. **61**, 813 (1987).

[17] B. Chen, I. Siepmann, and M. L. Klein, J. Phys. Chem. B **105**, 9840 (2001).